

From Pixels to Histopathology: A Graph-Based Framework for Interpretable Whole Slide Image Analysis

Alexander Weers^{1,3}, Alexander H. Berger^{1,6}, Laurin Lux^{1,3,6}, Peter Schüffler^{3,5},
Daniel Rueckert^{1,2,3,4}, and Johannes C. Paetzold^{2,6}

¹ School of Computation, Information and Technology, Technical University of
Munich, DE

² Department of Computing, Imperial College London, UK

³ Munich Center of Machine Learning, DE

⁴ Munich Data Science Institute, Technical University of Munich, Munich, DE

⁵ Institute of Pathology, TUM School of Medicine and Health, Technical University
of Munich, Munich, Germany

⁶ Weill Cornell Medicine, Cornell University, New York City, NY, USA
`alexander.weers@tum.de;jpaetzold@med.cornell.edu`

Abstract. The histopathological classification of whole-slide images (WSIs) is a fundamental task in digital pathology; yet it requires extensive time and expertise from specialists. While deep learning methods show promising results, they typically process WSIs by dividing them into artificial patches, which inherently prevents a network from learning from the entire image context, disregards natural tissue structures and compromises interpretability. Our method overcomes this limitation through a novel graph-based framework that constructs WSI graph representations. The WSI-graph efficiently captures essential histopathological information in a compact form. We build tissue representations (nodes) that follow biological boundaries rather than arbitrary patches all while providing interpretable features for explainability. Through adaptive graph coarsening guided by learned embeddings, we progressively merge regions while maintaining discriminative local features and enabling efficient global information exchange. In our method’s final step, we solve the diagnostic task through a graph attention network. We empirically demonstrate strong performance on multiple challenging tasks such as cancer stage classification and survival prediction, while also identifying predictive factors using Integrated Gradients. Our implementation is publicly available at <https://github.com/HistoGraph31/pix2pathology>

Keywords: Graph Representation Learning · Whole Slide Image · Computational Pathology · Interpretable AI

1 Introduction

Cancer diagnosis and treatment planning depend on histopathological examination, with pathologists analyzing tissue samples to identify malignancies and

suggest optimal therapeutic strategies. This process has become increasingly challenging as cancer incidence continues to rise, with an estimated 20 million new cases and almost 10 million deaths annually. The growing demand for histopathological assessment, coupled with a worldwide shortage of specialists [19], has created an urgent need for computational tools that can augment and accelerate diagnostic workflows.

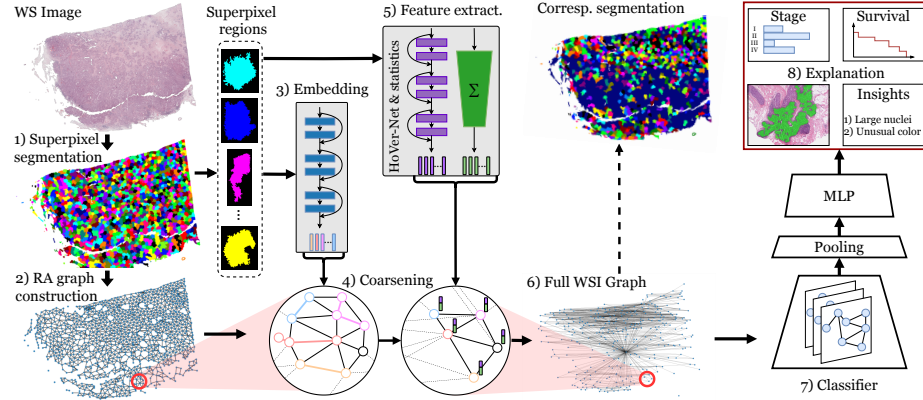


Fig. 1. Overview of our method for transforming Whole Slide Images (WSIs) into graph representations aligning with natural tissue borders. Starting from a WSI, superpixels are segmented by clustering pixels based on color and spatial proximity using SLIC (1). Region embeddings are obtained using a contrastively pretrained CNN (3), enabling similarity-based merging of adjacent nodes (4). Interpretable features (radiomics, region statistics, and nuclear characteristics) enrich each node resulting in a compact yet information-rich representation (6). Using this graph we train a graph attention network for the different diagnostic tasks (7). Through integrated gradients, the models predictions can be attributed to regions and features (8).

While recent advances in artificial intelligence have shown promise in automating histopathological analysis [26,22], significant challenges remain in processing Whole Slide Images (WSIs). These gigapixel-scale images, often exceeding $100,000 \times 100,000$ pixels, contain complex tissue architectures that pathologists carefully examine for diagnostic cues [29]. Current deep learning approaches typically address this excessive scale by dividing WSIs into small, rectangular patches - an artificial constraint that fragments natural tissue structures and loses important contextual information [7]. Moreover, these methods often fail to attribute their prediction to clear-defined areas or interpretable features.

We address these limitations by introducing a novel framework that transforms WSIs into biologically-informed graph representations. Our approach begins by identifying meaningful tissue regions through adaptive segmentation, preserving natural boundaries instead of imposing arbitrary divisions. These re-

gions become nodes in a graph structure, enriched with interpretable features that capture multi-scale tissue characteristics:

- Region-level features describing morphological and textural patterns [10]
- Cellular organization metrics derived from nuclear analysis [9]
- Learned embeddings that capture complex tissue appearance patterns

The graph structure explicitly models spatial relationships between regions while adaptively merging similar areas, integrating multi-scale information, that includes both local features and global (WS-level) spatial relationships. This approach offers several key advantages:

1. Preservation of biological structures through boundary-aware segmentation
2. Efficient compression of entire slides into an information-rich representation
3. Direct mapping between model predictions and interpretable tissue characteristics
4. Suitability for lightweight model architectures requiring minimal computational resources

Our experimental results demonstrate that this biologically-informed approach achieves strong performance across multiple histopathological tasks while providing clear explanations that align with clinical expertise. By combining Graph Attention Networks [30] with our interpretable representation, we enable efficient whole-slide analysis while maintaining transparency - a crucial step toward practical AI adoption in clinical pathology.

2 Related work

2.1 Histopathology classification

Histopathology slide classification has seen remarkable progress in recent years [27,24]. The extremely high resolution of whole-slide images (WSIs) makes direct processing computationally infeasible, leading to various strategies for efficient analysis. Multi-Instance Learning (MIL) [34] has emerged as a dominant paradigm, where slides are divided into patches processed individually, as demonstrated by ABMIL [14] and DSMIL [15]. Unlike these patch-based methods, our approach preserves natural tissue boundaries by utilizing adaptive region segmentation.

Recent work has focused on incorporating multi-scale information and improving computational efficiency, for instance, Xiong et al. [32] propose hierarchical MIL by integrating multiple magnification levels. Huang et al. [13] introduce training strategies that reduce computational requirements while enhancing feature quality. While these methods improve efficiency, they still rely on artificial patch boundaries that may not align with biological structures.

The field has recently seen the emergence of foundation models [5,31] and multimodal approaches incorporating genomic data [33]. However, these advancements often require massive computational resources, limiting their practical applicability. In contrast, our method achieves competitive performance even with limited data and modest computational requirements through an efficient graph-based representation.

2.2 Graph-Based Methods in Medicine

Graph-based learning methods have been successfully applied to many problems in medical AI, enhancing interpretability by capturing complex relationships in data [21,35,18]. In the context of whole slide image (WSI) analysis, graph-based representations offer a powerful alternative approach, providing advantages in computational efficiency, spatial structure modeling, and interpretability [3]. Existing methods typically construct graphs from image patches or segmented structures, where edges encode spatial or feature-based relationships. Some approaches focus on patch-level graph construction, such as Zheng et al. [36] who connect adjacent patch features using transformer-based models. HACT-Net [20] represents tissue components and cell nuclei as graph nodes but is limited to regions of interest rather than entire WSIs. Ramanathan et al. [23] utilize tissue segmentation for graph construction, while others explore selective patch sampling [2]. While these methods improve upon pure patch-based approaches, they either still rely on artificial patches or are limited in their scope. Recent developments in heterogeneous graph modeling include Chan et al. [4], who assign nuclei classification of HoverNet [9] as node classes, and Han et al. [11], who propose a multi-scale hypergraph approach for survival prediction.

3 Method

Our framework transforms gigapixel-scale whole-slide images (WSIs) into efficient, interpretable graph representations that preserve biological structures. Figure 1 illustrates our pipeline, which constructs adaptive regions and enriches them with interpretable features capturing multi-scale tissue characteristics.

3.1 Adaptive Region Segmentation

Given a whole-slide image (WSI) $\mathcal{I} \in \mathbb{R}^{H \times W \times 3}$, we first identify tissue regions \mathcal{T} using the tissue detection method from CLAM [17]. We then segment \mathcal{T} into K initial superpixels $\mathcal{S} = \{s_1, \dots, s_K\}$ using Simple Linear Iterative Clustering (SLIC) [1] on the lowest resolution level (magnification = 0.625x). Unlike rigid patch-based approaches, SLIC adapts to local tissue structures by clustering pixels based on color and spatial proximity.

Contrastive Region Embeddings We encode each region into a high-dimensional embedding space using a pretrained CNN model $h_j = \psi_{\text{CNN}}(s_j) \in \mathbb{R}^{512}$. The model ψ_{CNN} was pretrained [36] on histological image patches using contrastive learning [6], enabling it to capture general tissue appearance patterns.

Adaptive Region Merging We coarsen the graph representation through an adaptive region merging process that preserves biological structures while reducing computational complexity. Adjacent regions s_j and s_k are merged if their contrastive region embeddings similarity exceeds a threshold τ . This process creates larger regions in homogeneous tissue areas while maintaining fine-grained segmentation in heterogeneous regions. Thereby, the initial superpixel set \mathcal{S} is compressed into the adaptively merged set \mathcal{S}_{AM} with $|\mathcal{S}_{AM}| < |\mathcal{S}|$. Opposed to other coarsening approaches, e.g. SLIC, our adaptive region merging guarantees that only areas with very similar tissue characteristics are combined. This stands in contrast to SLIC-based merging which only considers color and location information.

This two-step approach of first segmenting superpixels and then merging them based on their embeddings ensures a low computational complexity while also capturing larger tissue regions, despite variations in color and brightness.

3.2 Interpretable Feature Extraction

We complement the graph structure with a curated subset of domain-informed features $x_j = [x_j^{\text{rad}} \mid x_j^{\text{stat}} \mid x_j^{\text{nuc}}]$ that correspond to clinically relevant tissue characteristics. After extracting the full feature set, we performed correlation analysis to eliminate redundant features, retaining only those with minimal inter-correlation. We can distinguish three groups of features:

- $x_j^{\text{rad}} \in \mathbb{R}^{93}$: **Radiomics features** [10] capturing texture patterns, shape descriptors, and intensity distributions
- $x_j^{\text{stat}} \in \mathbb{R}^{21}$: **Region statistics** including size and color distributions in multiple color spaces (RGB, LAB, HSV)
- $x_j^{\text{nuc}} \in \mathbb{R}^{77}$: **Nuclear characteristics** derived from HoVerNet [9], including density and size statistics for six nuclei types

WSI Graph Representation The background region $\mathcal{B} = \mathcal{I} \setminus \mathcal{F}$ is assigned zero-valued feature vectors, ensuring consistent graph connectivity while clearly distinguishing them from tissue regions. The WSI is represented as a graph $\mathcal{G}_{WSI} = (\mathcal{V}_{WSI}, \mathcal{E}_{WSI})$ where:

- Nodes $v_j \in \mathcal{V}_{WSI}$ represent tissue regions with feature vectors x_j . Each node v_j corresponds to a tissue region $S_{j,AM} \in \mathcal{S}_{AM}$.

Table 1. Performance comparison of different baselines and our method across two tasks on TCGA-BRCA (1133 WSIs). Best performance is **bold**, second best underlined, and statistical significance (p -value < 0.05) compared to our method is indicated with an *. UNI2 is trained on an extra 350 000 WSIs compared to all other methods.

| Method | Stage Classification | | | Survival Prediction |
|------------------|----------------------|----------------------------|-------------------------|---------------------|
| | AUC \uparrow | F1 _m \uparrow | Balanced Acc \uparrow | C-Index \uparrow |
| DeepSets | 52.3* (3.05) | 15.8* (5.50) | 25.4 (0.10) | 48.9* (2.47) |
| ABMIL | 61.8* (5.64) | 20.2* (2.13) | 26.0 (1.11) | 61.7 (1.81) |
| GraphTransformer | 63.3 (2.33) | 18.6* (0.89) | 24.9 (0.14) | 52.7* (5.61) |
| UNI2-h | 69.8 (3.05) | 30.1 (4.45) | 31.0* (2.78) | <u>62.1</u> (6.90) |
| Ours | <u>67.2</u> (3.08) | <u>28.0</u> (8.24) | <u>27.0</u> (2.54) | 62.9 (3.67) |

- Edges $(v_j, v_k) \in \mathcal{E}_{WSI}$ connect spatially adjacent regions. Edges are introduced when two pixels p corresponding to separate superpixels are adjacent. $(v_j, v_k) = 1 \iff \exists p_a \in S_{j,AM}, p_b \in S_{k,AM}$ such that $\text{Adj}(p_a, p_b) = 1$

This graph representation effectively captures both local tissue characteristics and global structural relationships, while being significantly more compact than the original WSI. By combining adaptive regions with interpretable features, it facilitates efficient learning and provides biologically meaningful explanations.

4 Results & Discussion

Table 2. Performance comparison of different baselines and our method across two tasks on TCGA-UCEC (566 WSIs). Best performance is **bold**, second best underlined and statistical significance (p -value < 0.05) compared to our method is indicated with an *. UNI2 is trained on an extra 350 000 WSIs compared to all other methods.

| Method | Stage Classification | | | Survival Prediction |
|------------------|----------------------|----------------------------|-------------------------|---------------------|
| | AUC \uparrow | F1 _m \uparrow | Balanced Acc \uparrow | C-Index \uparrow |
| DeepSets | 49.4* (1.48) | 9.46* (6.47) | 24.4 (1.67) | 50.3* (0.60) |
| ABMIL | 49.0* (2.61) | 18.8 (0.00) | 25.0 (0.00) | 58.3 (5.31) |
| GraphTransformer | 54.1 (4.51) | 18.7 (1.18) | 25.2 (0.58) | 57.5 (7.84) |
| UNI2-h | 62.7* (5.03) | 28.0* (4.67) | 30.4* (2.92) | 62.8 (5.38) |
| Ours | <u>56.4</u> (4.17) | <u>19.5</u> (1.19) | <u>26.5</u> (2.37) | <u>60.0</u> (0.97) |

Table 1 and Table 2 present the performance comparison of our method against various baselines, including the foundation model UNI2-h [5]. We evaluate all models on two different datasets, each on two tasks: stage classification and survival prediction, on the TCGA-BRCA [16] and TCGA-UCEC [8]

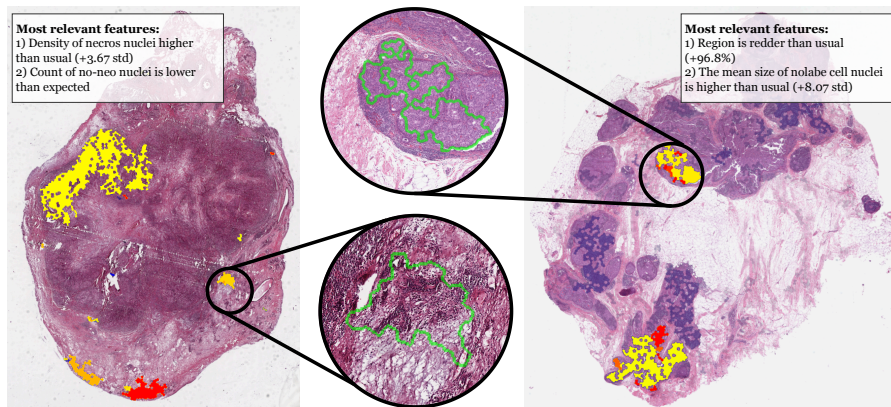


Fig. 2. Examples (both: cancer stage 2) of the attribution to the most influential tissue regions for the staging decision for two WSIs of TCGA-BRCA. Red to blue indicates decreasing relevance. Only the most important tissue regions are marked with an overlay. Moreover, the text boxes describe decisive tissue characteristics for the model decision.

datasets. For each dataset, we separate a fixed test set for evaluation and perform 5-fold cross-validation for model selection on the remaining data.

TCGA-BRCA performance Our method outperforms all non-foundational models on stage classification and survival prediction on the TCGA-BRCA dataset. We see statistically significant performance improvements over DeepSets, ABMIL and GraphTransformer on numerous metrics. The large-scale pre-trained (350k WSIs) UNI2-h base model performs best in the stage classification task. Notably, often with small performance gains that are not statistically significant. In the survival prediction task, our method achieves the highest C-index even surpassing the UNI2-h foundation model.

TCGA-UCEC performance On the considerably smaller TCGA-UCEC dataset, our model yields the highest performance in stage classification and survival prediction among all standard methods. Compared to the TCGA-BRCA dataset the UNI2-h foundation model has a more distinct performance increase. We attribute this difference to the smaller dataset, where the pretraining advantages of foundation models are more distinct.

Comparison to UNI2-h Despite UNI2-h’s strong results, it is crucial to contextualize its advantages. UNI2-h is a foundation model trained on more than 200 million images from more than 350k images, requiring an order of magnitude more computational resources than our approach. Given the relatively modest performance gap, particularly in survival prediction, it is reasonable to expect

that our method could achieve comparable results with a similar scale of pre-training. Furthermore, the lack of statistical significance in many of UNI2-h’s improvements on TCGA-BRCA suggests that our method already provides a highly competitive alternative, particularly in resource-constrained settings.

Overall, our method consistently and substantially outperforms all models that are not trained on additional data across all datasets and tasks while closing the gap to foundation models.

Computational Efficiency Our method reaches competitive classification accuracy while maintaining significant computational advantages over current approaches. While the UNI foundation model achieves a slightly higher accuracy on the BRCA dataset, this comes at substantial computational and data costs.

- Training data volume: Ours (1K WSIs) vs UNI (350K+ 1K WSIs)
- Model size: Ours (164 kB) vs UNI (2.7GB)

4.1 From Model Predictions to Clinical Insights

A key advantage of our method is its ability to provide interpretable explanations through Integrated Gradients [28] that align with pathological assessment practices. Figure 2 highlights regions that are highly important for the prediction, along with their corresponding feature importance scores. In the left tumor sample, the model’s prediction is highly driven by the increased density of Necrotic (necros) nuclei and the absence of non-Neoplastic (no-neo) nuclei in the highlighted regions. This closely aligns with clinical practice, as pathologists routinely use these features for grading.[12,25]. In the second example the mean size of unlabeled nuclei (no-label) is one of the most important features for the classification, showing that our method utilizes a rich set of interpretable features. We provide a full list of features in our public repository.

In the future, this attribution to interpretable features will allow a direct comparison of the reasoning behind predictions with clinical guidelines and enable validation by domain experts. Furthermore, our region-based approach provides a clearer delineation of relevant areas compared to traditional heat map or integrated gradient visualizations.

5 Conclusion

We presented a novel framework for whole-slide image analysis that combines computational efficiency and biological interpretability. By constructing hierarchical tissue representations that follow natural boundaries rather than artificial patches, our method maintains crucial histological context while enabling efficient processing of gigapixel-scale images. The combination of adaptive region segmentation with interpretable feature extraction provides pathologists with insights that directly map to their diagnostic workflow, offering clear delineation

of relevant regions and quantifiable tissue characteristics.

Our experimental results demonstrate that this biologically-informed approach achieves competitive performance across multiple histopathological tasks without requiring the massive datasets and computational resources of recent foundation models. We argue that our method’s ability to adaptively adjust region granularity based on tissue complexity proves particularly valuable in heterogeneous areas such as tumor boundaries, where precise region delineation is crucial for accurate diagnosis.

In the future, we aim to perform large-scale clinical validation of our model explanations as in an expert reader study. Further, the interpretable nature of our region-based features could facilitate the integration of clinical guidelines into model training, potentially leading to more robust and clinically aligned predictions.

References

1. Achanta, R., Shaji, A., Smith, K., Lucchi, A., Fua, P., et al.: Slic superpixels compared to state-of-the-art superpixel methods. *IEEE Transactions on Pattern Analysis and Machine Intelligence* **34**(11), 2274–2282 (2012)
2. Adnan, M., Kalra, S., Tizhoosh, H.R.: Representation learning of histopathology images using graph neural networks. In: *CVPR Workshops*. pp. 988–989 (2020)
3. Brussee, S., Buzzanca, G., Schrader, A.M., Kers, J.: Graph neural networks in histopathology: Emerging trends and future directions. *Medical Image Analysis* **101** (2025)
4. Chan, T.H., Cendra, F.J., Ma, L., Yin, G., Yu, L.: Histopathology Whole Slide Image Analysis with Heterogeneous Graph Representation Learning . In: *CVPR*. pp. 15661–15670 (2023)
5. Chen, R.J., Ding, T., Lu, M.Y., Williamson, D.F.K., Jaume, G., et al.: Towards a general-purpose foundation model for computational pathology. *Nature Medicine* **30**(3), 850–862 (2024)
6. Chen, T., Kornblith, S., Norouzi, M., Hinton, G.: A simple framework for contrastive learning of visual representations. In: *Proceedings of the 37th International Conference on Machine Learning. ICML’20* (2020)
7. Ciga, O., Xu, T., Nofech-Mozes, S., Noy, S., Lu, F.I., et al.: Overcoming the limitations of patch-based learning to detect cancer in whole slide images. *Scientific Reports* **11**(1), 8894 (2021)
8. Erickson, B.J., Mutch, D., Lippmann, L., Jarosz, R.: The cancer genome atlas uterine corpus endometrial carcinoma collection (TCGA-UCEC) (2016). <https://doi.org/10.7937/K9/TCIA.2016.GKJ0ZWAC>
9. Graham, S., Vu, Q.D., Raza, S.E.A., Azam, A., Tsang, Y.W., et al.: Hover-net: Simultaneous segmentation and classification of nuclei in multi-tissue histology images. *Medical Image Analysis* **58**, 101563 (2019)
10. van Griethuysen, J.J.M., Fedorov, A., Parmar, C., Hosny, A.a.: Computational radiomics system to decode the radiographic phenotype. *Cancer Res* **77**(21) (2017)
11. Han, M., Zhang, X., Yang, D., Liu, T., Kuang, H., et al.: Multi-Scale Heterogeneity-Aware Hypergraph Representation for Histopathology Whole Slide Images . In: *ICME*. pp. 1–6 (2024)
12. Hayakawa, T., Prasath, V.S., Kawanaka, H., Aronow, B.J., Tsuruoka, S.: Computational nuclei segmentation methods in digital pathology: a survey. *Archives of Computational Methods in Engineering* **28**, 1–13 (2021)
13. Huang, W., Hu, X., Abousamra, S., Prasanna, P., Chen, C.: Hard negative sample mining for whole slide image classification. In: *MICCAI*. pp. 144–154 (2024)
14. Ilse, M., Tomczak, J., Welling, M.: Attention-based deep multiple instance learning. In: *International conference on machine learning*. pp. 2127–2136. PMLR (2018)
15. Li, B., Li, Y., Eliceiri, K.W.: Dual-stream multiple instance learning network for whole slide image classification with self-supervised contrastive learning. In: *CVPR*. pp. 14318–14328 (2021)
16. Lingle, W., Erickson, B.J., Zuley, M.L., Jarosz, R., Bonaccio, E., et al.: The cancer genome atlas breast invasive carcinoma collection (TCGA-BRCA) (2016). <https://doi.org/10.7937/K9/TCIA.2016.AB2NAZRP>
17. Lu, M.Y., Williamson, D.F., Chen, T.Y., Chen, R.J., Barbieri, M., et al.: Data-efficient and weakly supervised computational pathology on whole-slide images. *Nature Biomedical Engineering* **5**(6), 555–570 (2021)

18. Lux, L., Berger, A.H., Tricas, M.R., Fayed, A.E., Sivaprasada, S., et al.: Interpretable retinal disease prediction using biology-informed heterogeneous graph representations (2025)
19. Metter, D.M., Colgan, T.J., Leung, S.T., Timmons, C.F., Park, J.Y.: Trends in the us and canadian pathologist workforces from 2007 to 2017. *JAMA Network Open* **2**(5), e194337–e194337 (2019)
20. Pati, P., Jaume, G., Foncubierta-Rodriguez, A., et al.: Hierarchical graph representations in digital pathology. *Medical Image Analysis* **75**, 102264 (2022)
21. Qiu, X., Wang, F., Sun, Y., Lian, C., Ma, J.: Towards graph neural networks with domain-generalizable explainability for fmri-based brain disorder diagnosis. In: *MICCAI*. pp. 454–464 (2024)
22. Raciti, P., Sue, J., Retamero, J.A., Ceballos, R., Godrich, R., et al.: Clinical validation of artificial intelligence-augmented pathology diagnosis demonstrates significant gains in diagnostic accuracy in prostate cancer detection. *Archives of Pathology & Laboratory Medicine* **147**(10), 1178–1185 (2023)
23. Ramanathan, V., Pati, P., McNeil, M., Martel, A.L.: Ensemble of prior-guided expert graph models for survival prediction in digital pathology. In: *MICCAI* (2024)
24. Shmatko, A., Ghaffari Laleh, N., Gerstung, M., Kather, J.N.: Artificial intelligence in histopathology: enhancing cancer research and clinical oncology. *Nature Cancer* **3**(9), 1026–1038 (2022)
25. Singletary, S.E., Connolly, J.L.: Breast cancer staging: Working with the sixth edition of the ajcc cancer staging manual. *CA: A Cancer Journal for Clinicians* **56**(1), 37–47 (2006)
26. Song, A.H., Jaume, G., Williamson, D.F.K., Lu, M.Y., Vaidya, A., et al.: Artificial intelligence for digital and computational pathology. *Nature Reviews Bioengineering* **1**(12), 930–949 (2023)
27. Srinidhi, C.L., Ciga, O., Martel, A.L.: Deep neural network models for computational histopathology: A survey. *Medical Image Analysis* **67**, 101813 (2021)
28. Sundararajan, M., Taly, A., Yan, Q.: Axiomatic attribution for deep networks. In: *ICML*. pp. 3319–3328 (2017)
29. Tseng, L.J., Matsuyama, A., MacDonald-Dickinson, V.: Histology: The gold standard for diagnosis? *Can Vet J* **64**(4), 389–391 (2023)
30. Velickovic, P., Cucurull, G., Casanova, A., Romero, A., Lio, P., et al.: Graph attention networks. *stat* **1050**(20), 10–48550 (2017)
31. Wang, X., Zhao, J., Marostica, E., Yuan, W., Jin, J., et al.: A pathology foundation model for cancer diagnosis and prognosis prediction. *Nature* **634** (2024)
32. Xiong, C., Chen, H., Sung, J.J., King, I.: Diagnose like a pathologist: Transformer-enabled hierarchical attention-guided multiple instance learning for whole slide image classification. In: *IJCAI-23*. pp. 1587–1595 (2023)
33. Xiong, C., Chen, H., Zheng, H., Wei, D., et al.: Mome: Mixture of multimodal experts for cancer survival prediction. In: *MICCAI*. pp. 318–328 (2024)
34. Zaheer, M., Kottur, S., Ravanbakhsh, S., Póczos, B., Salakhutdinov, R.R., et al.: Deep sets. *Advances in neural information processing systems* **30** (2017)
35. Zheng, S., Zhu, Z., Liu, Z., Guo, Z., Liu, Y., Yang, Y., Zhao, Y.: Multi-modal graph learning for disease prediction. *IEEE Transactions on Medical Imaging* **41**(9), 2207–2216 (2022)
36. Zheng, Y., Gindra, R.H., Green, E.J., Burks, E.J., Betke, M., et al.: A graph-transformer for whole slide image classification. *IEEE transactions on medical imaging* **41**(11), 3003–3015 (2022)